Noncovalent Interactions in Crystalline Picolinic Acid N-Oxide: Insights from Experimental and Theoretical Charge Density Analysis

ARTICLE *in* CRYSTAL GROWTH & DESIGN · JANUARY 2013

Impact Factor: 4.89 · DOI: 10.1021/cg3015223

6 AUTHORS, INCLUDING:

Anastasia V. Shishkina
Mendeleev Russian University of Chemical Tec…
8 PUBLICATIONS **97** CITATIONS
SEE PROFILE

Adam I. Stash
Karpov Institute of Physical Chemistry
169 PUBLICATIONS **1,290** CITATIONS
SEE PROFILE

Mikhail V Vener
Mendeleev Russian University of Chemical Tec…
69 PUBLICATIONS **1,171** CITATIONS
SEE PROFILE

Vladimir G Tsirelson
Mendeleev Russian University of Chemical Tec…
172 PUBLICATIONS **1,926** CITATIONS
SEE PROFILE

CRYSTAL GROWTH & DESIGN

Article

pubs.acs.org/crystal

Noncovalent Interactions in Crystalline Picolinic Acid N-Oxide: Insights from Experimental and Theoretical Charge Density Analysis

Anastasia V. Shishkina,[†] Vladimir V. Zhurov,[‡] Adam I. Stash,[†,§] Mikhail V. Vener,[†] A. Alan Pinkerton,[‡] and Vladimir G. Tsirelson*[,†]

[†]Mendeleev University of Chemical Technology, 9, Miusskaya Square, 125047 Moscow, Russia

[‡]Department of Chemistry, University of Toledo, Toledo, Ohio 43606, United States

[§]Karpov Institute of Physical Chemistry, 10, Vorontsovo Pole, 105064 Moscow, Russia

Supporting Information

ABSTRACT: This study provides a detailed description of noncovalent interactions of different types and strengths in the title crystal using a combined experimental and theoretical study of the charge density distribution. The nature of the noncovalent interactions is visualized using information theory and through the superposition of the gradient fields in the electron density and electrostatic potential. The energy of the intramolecular O−H···O bond, intermolecular C−H···O bonds, and π-stacking interactions, E_{int}, are evaluated from empirical correlations between E_{int} and geometrical and electron-density bond critical point parameters. The complete set of noncovalent interactions including the strong intramolecular O−H···O (E_{int} > 90 kJ/mol) and weak C−H···O (E_{int} < 10 kJ/mol) hydrogen bonds, and π-stacking interactions (E_{int} < 4 kJ/mol) is quantitatively described. The results from the experimental charge density analysis are compared with periodic quantum calculations using density functional theory with the Grimme dispersion correction. It was found that the Grimme dispersion correction did not provide a good simultaneous description of both weak and strong noncovalent interactions in the studied crystal. It is shown that the obtained energies of noncovalent interactions lead to a reasonable value of the lattice energy. The latter is treated as the total intermolecular interaction energy.

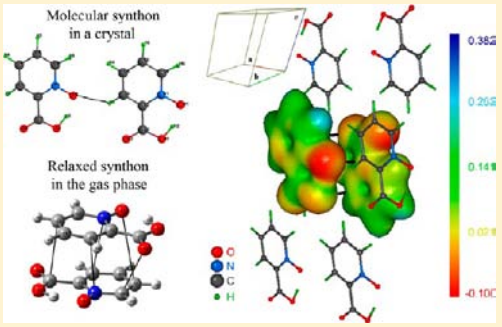

1. INTRODUCTION

Accurate determination of the energy of noncovalent interactions in crystals and decomposition of this energy into different components are important in many applications such as crystal engineering,[1] the development of pharmaceutical products[2] and optical materials.[3] Experiments provide the sublimation enthalpy, a global measure of intermolecular interactions in a crystal, at a given temperature, which can be extrapolated to 0 K, ΔH°_{sub}.[4] The corresponding theoretical value of the lattice energy E_{latt} at T = 0 K can be evaluated using periodic density functional methods with an *a posteriori* empirical correction for the dispersion interactions (DFT-D)[5] or a periodic full *ab initio* quantum mechanical method based on Møller−Plesset perturbation theory for the electron correlation.[6] For molecular crystals this energy is[5,7]

$$E_{latt} = E(\text{bulk})/Z - E(\text{mol}) \quad (1)$$

E(bulk) is the total energy of the unit cell, which includes Z molecules, and E(mol) is the total energy of the isolated gas-phase molecule calculated at the same level of theory. Unfortunately, decomposition of both ΔH°_{sub} and E_{latt}, the cumulative characteristics of molecular interactions in crystals, into the specific atom−atom or molecule−molecule components is usually impossible. However, the application of eq 1 to cocrystals and crystal solvates, is not straightforward. This is why different approximate schemes for the evaluation of E_{latt} are commonly used; for example, see refs 7a and 8. Specifically, in the rigid-molecule approximation, the lattice energy is equated to the total intermolecular interaction energy of a crystal.[8b] If many-body contributions to the intermolecular energy[9] are ignored,[8a,b] this quantity can be presented as a sum of the pairwise interactions, E'_{latt}. Therefore, for the sublimation enthalpy of a molecular crystal reduced to 0 K,[7a,8a] we can write

$$E'_{latt} = \Delta H^{0}_{sub} = \sum_{j} \sum_{j<i} E_{int,j,i} \quad (2)$$

Here $E_{int,j,i}$ is the energy of a particular intermolecular (noncovalent) interaction between pairs of atoms i and j belonging to different molecules (for simplicity, we consider the case for Z' = 1). Values of $E_{int,j,i}$ are commonly determined by (i) the atom−atom potential method,[8c,10] (ii) the PIXEL method based on empirical partitioning of the interaction energy,[11] and (iii) a method exploring the linear relationships between $E_{int,j,i}$ and the electron-density features at the

Received: October 17, 2012
Revised: December 22, 2012
Published: January 11, 2013

   dx.doi.org/10.1021/cg3015223 | *Cryst. Growth Des.* 2013, 13, 816−828

noncovalent bond critical points (BCPs) in the electron density, notions derived from the quantum theory of atoms in molecules and crystals (QTAIMC[12]).[13] The attractive features of the latter approach are a uniform description of various kinds of intermolecular interactions defining the structure of molecular crystals[14] and a possibility to use both experimental and theoretical electron densities derived from precise X-ray diffraction experiments,[15] and DFT-D computations of a crystal with periodic boundary conditions (3D solid-state DFT calculations).[16]

The crystalline α-form of picolinic acid N-oxide (PANO) is a good subject for a consistent study of different noncovalent interactions, *viz* strong intramolecular O−H···O bonds,[17] relatively weak intermolecular C−H···O bonds,[17b] and weak π-stacking interactions. The intramolecular O−H···O bond in PANO was the subject of several previous studies.[17] In particular, the infrared, Raman and inelastic neutron scattering spectra of the crystal were evaluated using a Car−Parrinello molecular dynamics simulation.[17c] However, the electron density features and intermolecular interactions in the PANO crystal have not been previously studied.

In this work, we identify and quantify the pattern of noncovalent interactions in crystalline α-PANO using the electron density features reconstructed from both a precise X-ray diffraction experiment at 100 K and periodic 3D solid-state DFT-D calculations taking into account the Grimme empirical dispersion correction.[18] The energy of the intermolecular interactions was estimated using empirical correlations between $E_{int,j,i}$ and the QTAIMC electron-density parameters at the corresponding intermolecular BCPs. To validate the applicability of these correlations to the π-stacking interactions, the interaction energy was evaluated from periodic DFT calculations as the interlayer interaction energy of {010} slabs. We also report the electrostatic-potential features revealing a picture of the attractive electrostatic interactions between the molecules in crystalline PANO as seen from the QTAIMC approach.

There is an important practical aspect of accurate determination of the energy of noncovalent interactions in crystals. These interactions are often studied using the cluster approximation based on *ab initio* or DFT calculations of clusters (dimers, trimers, tetramers, etc.) for the cluster geometry extracted from a crystal.[19] Also to get more insight into the physical nature of the interaction, different interaction-energy decomposition schemes are used[20] or symmetry-adapted perturbation-theory is applied.[21] Unfortunately, these schemes do not allow us to extract the energy of the particular noncovalent interactions in molecular crystals and periodic systems, especially when several interactions of different kinds are involved. Moreover, although in some cases *ab initio* studies of molecular interactions using gas-phase clusters give reasonable results, in general this is not the case due to ignoring long-range interactions and related crystal-packing effects. The latter is also valid for studies based on the electron-density parameters at the BCPs.[19b,f,j,o,22] Therefore, it is important to clarify the specificity of using the BCP parameters derived within the gas-phase cluster model for characterization of noncovalent interactions in molecular crystals, as well as *vice versa*. We have considered this problem in detail.

2. EXPERIMENTAL SECTION

2.1. Data Collection and Reduction. Colorless single crystals of picolinic acid N-oxide were grown by slow evaporation of a saturated aqueous solution. Many of the crystals showed a significant amount of disorder accompanied by strong broadening of reflections along the direction of the powder rings. For data collection, a crystal without such broadening was carefully chosen. Nevertheless, a small amount of diffuse scattering was still observed especially for the strongest (020) reflection. The ratio of the Bragg peak intensity to the diffuse one was over 2000, and the diffuse peak was much broader. We thus estimated the diffuse contribution to the integration area to be less than 0.05% of the Bragg contribution, and considered it to be negligible. The data were collected using a Rigaku diffractometer equipped with an ULTRAX-18 rotating anode generator operated at 50 kV, 200 mA, and a RAPID cylindrical image plate detector. An Oxford Cryosystem cooler was used to maintain the temperature of the crystal at 100.0(1) K during data collection. The crystal size of 0.22 × 0.27 × 0.40 mm allowed the accumulation of 430 000 counts for the strongest peak using 120 s, 6° oscillation range images. Data collection consisted of 14 runs, each covering a 180° oscillation range, and collected at different goniostat settings (χ = 0°, φ = 0,180°; χ = 20,30,40°, φ = 0,90,180,270°). Each run consisted of 59 frames overlapped by half a frame width. Data were indexed with HKL2000[23] and integrated with VIIPP[24] using experimental peak profiles accumulated over all images and applied for reflections with intensity lower than 6 e.s.d.s. The obtained peak intensities corrected for Lorentz and polarization factors were then scaled and averaged with the program SORTAV.[25] Details of the experiment are given in Table 1.

Table 1. Crystallographic Data and Experimental Details for $C_6H_5NO_3$

chemical formula	$C_6H_5NO_3$
crystal system	monoclinic
space group	$P2_1/m$
a (Å)	6.7970(4)
b (Å)	6.0349(4)
c (Å)	7.7927(4)
β (deg)	112.610(4)
volume (Å^3), Z	295.08(3), 2
T (K)	100.0(1)
wavelength, λ (Å)	0.71073 (Mo Kα)
crystal size (mm)	0.22 × 0.27 × 0.40
$(\sin\theta/\lambda)_{max}$ (Å^{-1})	1.2
reflections integrated	113014
R_{int}/average data multiplicity	0.0167/25.4
completeness: $\sin\theta/\lambda$ < 0.75 Å^{-1}, all data, %	100, 98.9
independent reflections	4456
observed reflections ($I > 3\sigma$)	3225
Spherical-atom model, harmonic atomic displacements	
R_1, wR_2, GOF	0.0383, 0.1157, 1.13
$\Delta\rho_{min/max}$, e Å^{-3}	−0.31/0.74
Multipole model, anharmonic atomic displacements	
R_1, wR_2, GoF	0.0152, 0.0164, 1.36
weighting scheme: a, b[a]	0.006, 0.0033
$\Delta\rho_{min/max}$, e Å^{-3} all data, sin θ/λ < 1.0 Å^{-1}	−0.124/0.195, −0.088/0.144

[a] $w_2 = 1/\{\sigma^2(F^2) + (ap)^2 + bp\}$, $p = 0.3333F^2_{obs} + 0.6667F^2_{calc}$.

2.2. Charge Density Model Refinement. The structure was resolved by direct methods,[26] and the F^2-refinement of the independent atom model was conducted with SHELXL97.[27] Structure factors for symmetry-allowed reflections in space group $P2_1/m$ ($\sin\theta/\lambda \le 1.2$ Å^{-1}) were then used in the refinement of the Hansen-Coppens multipole model[28] restricted to the hexadecapole level for non-hydrogen atoms and the quadrupole level for hydrogen atoms. Fourth-order anharmonicity parameters were refined for non-hydrogen atoms to adequately describe the atomic displacements. The multipole model refinement based on F was carried out with the program XD2006.[29] First, the atomic positions and displacement parameters, scale factor

dx.doi.org/10.1021/cg3015223 | Cryst. Growth Des. 2013, 13, 816−828

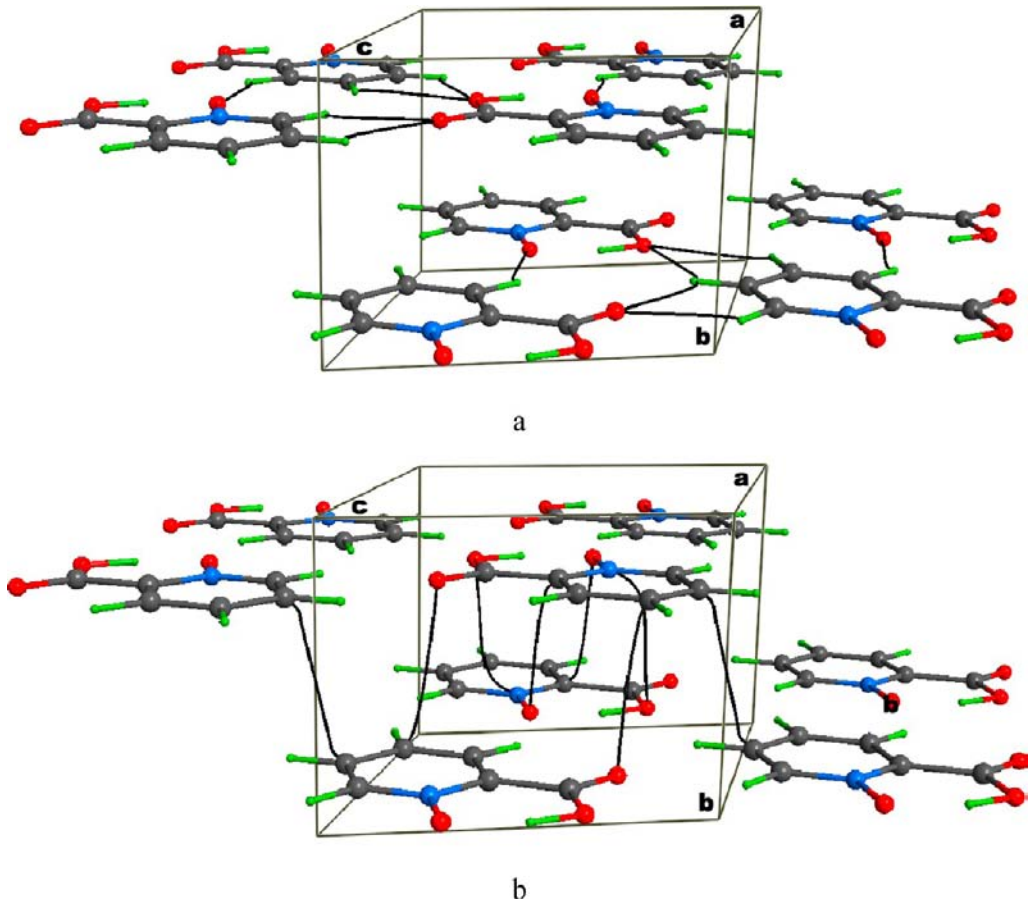

b

Figure 1. The molecular structure of the monoclinic PANO crystal. The black lines show the intermolecular bond paths: (a) intrasheet C−H···O contacts; (b) intersheet π-stacking contacts.

and multipole parameters for all the atoms were refined in the range sin $\theta/\lambda \leq 1.2$ Å^{-1} with fixed monopoles (P_v) and radial expansion/contraction parameters κ' and κ'' for all atoms (1.0 for all non-hydrogen atoms and 1.2 for hydrogen atoms). After convergence, the anharmonic displacement parameters were fixed and all other model parameters were refined. In the final stage the anharmonic displacement parameters were added to the refinement again with the exception of the oxygen atoms whose anharmonic parameters were found to be highly correlated with the corresponding κ' and κ'' coefficients. They were therefore fixed to the values obtained when κ' and κ'' were equal to 1.0. The electroneutrality condition was imposed throughout all the refinements.

The refinement details are listed in Table 1. The multipole model and atomic positional and displacement parameters have been deposited together with residual density maps. The molecular structure of the monoclinic PANO crystal is shown in Figure 1. The multipole parameters were used to calculate the quasi-static total and deformation densities (Figure 2). The total electron density was positive everywhere in space. The Laplacian of the experimental electron density was also calculated (Figure 3). Electron density properties at the BCPs[12a] were computed, and they are listed in Tables 2 and 3 and Table S2. For the closed-shell interactions, the kinetic (G_b) and potential (V_b) energies at the BCPs were also calculated from the electron density and its derivatives using the DFT formulas and the local virial theorem for equilibrium structures.[30] The atomic volumes, and atomic charges, integrated over atomic basins delimited by zero-flux surfaces, are listed in Table S3. All calculations were performed with the program WinXPRO.[31]

3. THEORETICAL

3.1. 3D Solid-State DFT Calculations. The DFT calculations were performed using the program CRYSTAL09.[32] B3LYP, BLYP, and PBE functionals were employed with an all-electron Gaussian-type localized orbital 6-311G(d,p) basis set and a Grimme modified empirical dispersion correction ($f(R)C_6/R^6$).[5,18a] The use of the modified B3LYP-D* model leads to better balanced results for both lattice constants and cohesive energies as well as for weakly hydrogen bonded and dispersion bonded molecular crystals. In contrast to plane-wave methods, the Gaussian-type orbital basis set enables computations with hybrid functionals like B3LYP. The default CRYSTAL09 options were employed for the Coulomb and Hartree−Fock exchange series accuracy level and for grid dimensions used for evaluating the DFT exchange-correlation contribution. The tolerance of the energy controlling the self-consistent field convergence for the geometry optimization and frequency computations was set to 1×10^{-9} and 1×10^{-10} hartree respectively. The number of points for the numerical first derivative calculations of the analytical nuclear gradients was chosen equal to 2. The shrinking factor of the reciprocal space grid was set to 4. The intramolecular O···O and intermolecular C−H···O distances, computed using the B3LYP/6-311G(d,p), BLYP/6-311G(d,p), and PBE/6-311G-(d,p) approximations with and without the Grimme dispersion correction, are given in Table S4. The B3LYP/6-311G(d,p) approximation was found to give the best results for the

dx.doi.org/10.1021/cg3015223 | Cryst. Growth Des. 2013, 13, 816−828

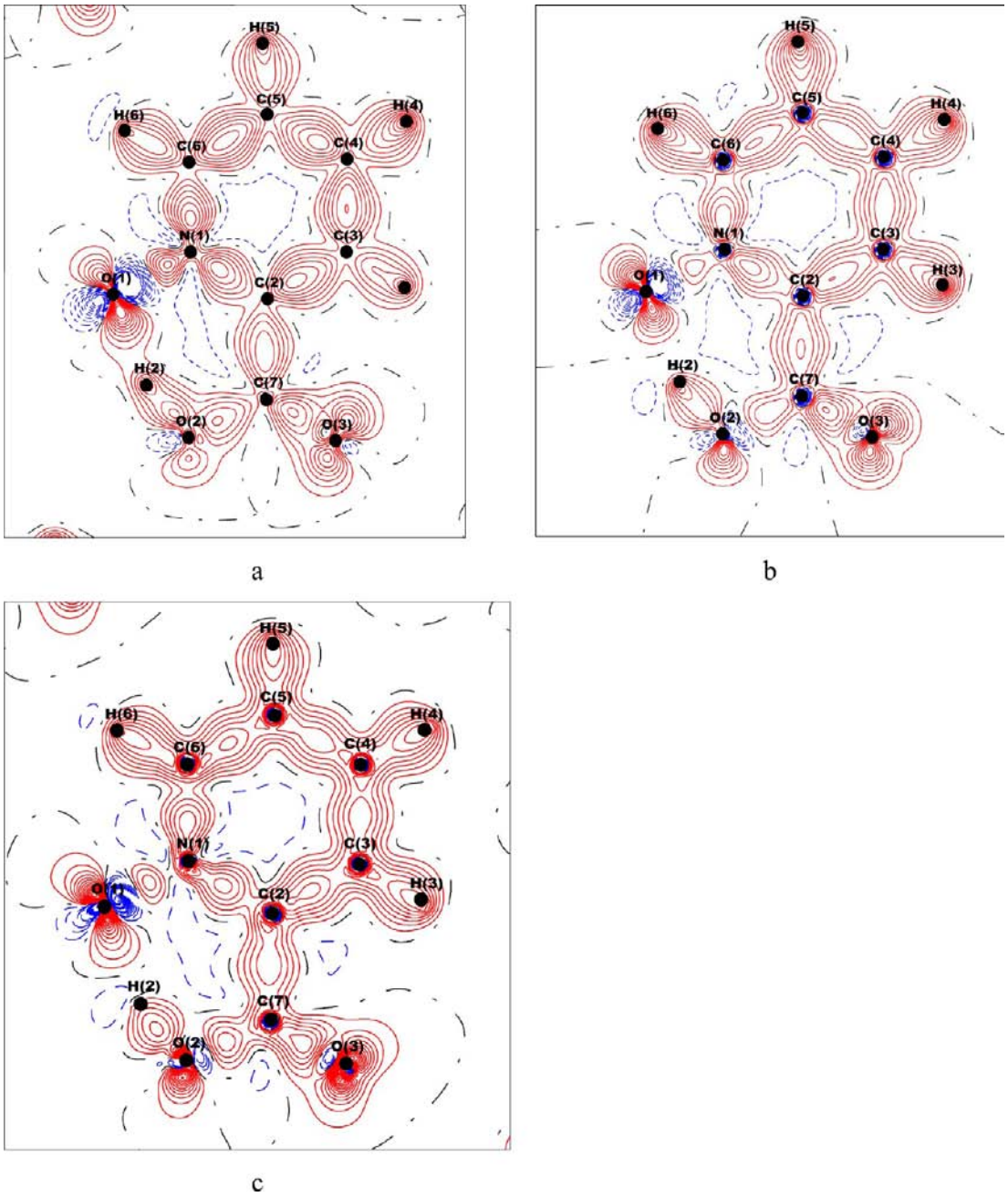

Figure 2. The deformation electron density in the (010) plane of crystalline PANO: (a) the model electron density derived from the X-ray diffraction experiment; (b) B3LYP-D*/6-311G(d,p) multipole model crystal calculation; (c) B3LYP-D*/6-311G(d,p) crystal calculation. Red and blue lines represent positive and negative DED values respectively. Contour intervals are 0.1 e Å^{-3}.

structural parameters of the present crystal. Therefore, it was used in the current study.

During the optimization, the unit cell parameters of the PANO crystal were fixed to the experimental values (Table 1), and structural relaxations were limited to variations in the atomic positional parameters allowed in space group $P2_1/m$. This approximation yields reasonable values for the harmonic IR frequencies and intensities obtained from the DFT computations of molecular crystals.[33] The experimental values of the atomic positions (Table S1) were used as the starting point for the DFT calculations. The vibrational frequencies computed at the Γ-point were found to be positive in all cases. Thus, the optimized crystal structure corresponds to the minimum on the potential energy surface. The comparison of the IR frequencies obtained from various levels of theory is given in Table 4.

3.2. Multipole Refinement Based on Theoretical X-ray Structure Factors. Static theoretical structure factors for PANO were calculated for all possible *hkl* indices up to $\sin\theta/\lambda \leq 1.2$ Å^{-1} using the XFAC module of the package CRYSTAL09. The same Hansen-Coppens multipole formalism[28] as for the refinement using experimental data was applied ($R(F) = 0.0045$). The atomic positions were fixed to those obtained from the energy minimization, and the refinement was carried out with unit weights. As a result, both experimental and theoretical electron densities were described with the same model suitable for further QTAIMC analysis. The deformation densities computed directly from the wave functions and

dx.doi.org/10.1021/cg3015223 | *Cryst. Growth Des.* 2013, 13, 816−828

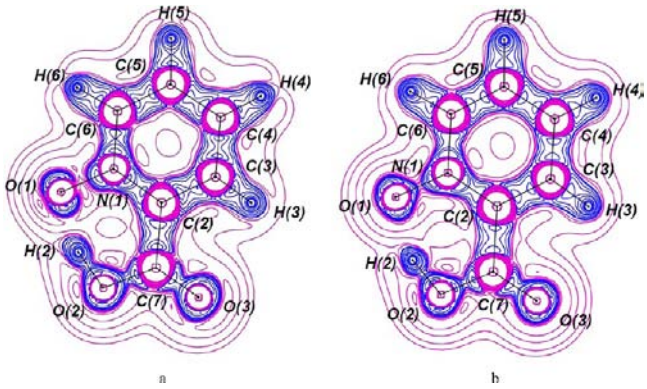

Figure 3. The Laplacian of the electron density in the (010) plane of crystalline PANO: (a) derived from the model electron-density from the X-ray diffraction experiment; (b) from the B3LYP-D*/6-311G(d,p) model calculation. Violet and blue lines represent positive and negative Laplacian values respectively. Line intervals are $\pm 2 \times 10^n$, $\pm 4 \times 10^n$, and $\pm 8 \times 10^n$ e Å^{-5} ($-2 \le n \le 2$).

obtained from the multipole model parameters are shown in Figure 2. The comparison of the other electron density characteristics is given in Tables 2, 3, and S5.

3.3. Energy of Noncovalent Interactions. Different empirical approaches have been used to estimate the energies of individual hydrogen bonds in molecular crystals using electron density,[22] geometrical[34] and spectral[35] parameters. For example, an empirical correlation between E_{int} (in kJ/mol) and the O···O distance (Å) has been suggested for intramolecular hydrogen bonds:[34c]

$$E_{int} = -23.255 \times 10^5 \exp(-4.12R(O\cdots O)) \quad (3)$$

This equation provides a successful estimation of the energy of intramolecular hydrogen bonds in the solid state.[34c,36]

Table 3. Experimental (First Line) and Theoretical B3LYP-D*/6-311G(d,p) with Grimme Dispersion Correction[a] (Second Line) Characteristics of the Intersheet π-Stacking Interactions in the PANO Crystal[b]

				E_{int}, kJ/mol	
contact	R, Å	$\rho(r)$	$\nabla^2\rho(r)$	c	d
C2···O1	3.211	0.006	0.023	3.9	4.5
	3.228	0.006	0.022	3.9	4.5
C6···O2	3.196	0.006	0.023	3.9	5.6
	3.202	0.006	0.024	3.9	4.5
C4···O3	3.314	0.004	0.016	2.6	3.4
	3.296	0.004	0.016	2.6	3.4
C3···C3	3.571	0.004	0.014	2.6	3.4
	3.614	0.003	0.013	1.3	2.3
C5···C5	3.291	0.006	0.020	3.9	4.5
	3.259	0.005	0.021	3.9	4.5

[a]Computations without Grimme dispersion correction give results which are similar to those obtained with Grimme dispersion correction. [b]R is the distance of the particular contact, electron density parameters derived from multipole refinement are given in a.u.. E_{int} is the energy of the contact evaluated using eqs 4 and 5. [c]Evaluated using eq 4. [d]Evaluated using eq 5.

Also, it has been suggested[22a] that the C−H···O hydrogen bonding energy, E_{int}, may be estimated using the electronic potential energy density, $V_b \equiv V(\mathbf{r}_b)$ at the H···O BCP, $\mathbf{r}_b$, in the electron density:[16j]

$$E_{int} = -0.5V_b \text{ (in atomic units)} \quad (4)$$

This equation is valid for weak and moderate hydrogen bonds (R(H···O) > 1.60 Å).[22a] Nevertheless, it has also been applied to crystals with strong bonds,[16g,37] and to noncovalent interactions other than hydrogen bonds[38] without any justification. A similar approach links the energy of the

Table 2. Experimental and Calculated Selected Geometrical and Electron-Density Parameters Derived from Multipole Refinement of the Intramolecular O−H···O Bond and Intrasheet C−H···O Contacts in PANO[a]

						E_{int}, kJ/mol		
contact, (X−H···O)		$R_{(X\cdots Y)}$, Å	$R_{(H\cdots Y)}$, Å	$\rho(r)$	$\nabla^2\rho(r)$	b	c	d
O1−H1···O2	exp	2.422	1.445	0.116	0.051	107.9		
	Grimme	2.466	1.495	0.082	0.181	90.0		
	opt	2.448	1.318	0.116	0.243	96.9		
C3−H3···O1	exp	3.228	2.397	0.009	0.039		7.9	9.0
	Grimme	3.230	2.355	0.010	0.045		7.9	10.1
	opt	3.404	2.418	0.009	0.038		7.9	9.0
C4−H4···O2	exp	3.421	2.778	***no BCP***				
	Grimme	3.374	2.713	0.004	0.023		3.9	4.5
	opt	3.464	2.797	0.005	0.020		2.6	4.5
C6−H6···O3	exp	3.076	2.310	0.010	0.051		9.2	11.3
	Grimme	3.065	2.338	0.010	0.053		9.2	11.3
	opt	3.068	2.342	0.011	0.048		9.2	11.3
C5−H5···O2	exp	3.313	2.591	0.006	0.029		5.3	6.8
	Grimme	3.324	2.627	0.005	0.028		3.9	5.6
	opt	3.248	2.606	0.007	0.028		5.3	5.6
C5−H5···O3	exp	3.277	2.683	***no BCP***				
	Grimme	3.217	2.599	0.005	0.031		3.9	6.8
	opt	3.380	2.642	0.006	0.027		5.3	5.6

[a]B3LYP/6-311G(d,p) computations with periodic boundary conditions were performed with (Grimme) and without (opt) Grimme dispersion correction. The energy of the contacts is given in the last columns. Electron density parameters are given in a.u. [b]Evaluated using eq 3. [c]Evaluated using eq 4. [d]Evaluated using eq 5.

dx.doi.org/10.1021/cg3015223 | Cryst. Growth Des. 2013, 13, 816−828

Table 4. Geometrical Parameters for the O2−H2···O1 Fragment (Å) for the Periodic and Gas-Phase Theoretical Model Obtained at Different Levels of Approximation[a]

method	$R_{(O2\cdots O1)}$, Å	$R_{(H2\cdots O1)}$, Å	$\rho(r)$, a.u.	OH_s frequency, cm^{-1}	E_{int}, kJ/mol
experiment	2.422	1.445	0.116		107.9
optimized crystal B3LYP-D*	2.466	1.494	0.070	2657	90.0
optimized crystal B3LYP	2.448	1.426	0.090	2564	96.9
optimized crystal PBE	2.432	1.403	0.109	2233	103.4
optimized crystal PBE-D*	2.463	1.459	0.092	2368	91.0
dimer model B3LYP-D*	2.529	1.582	0.067	2805	69.4

[a] E_{int} (kJ/mol) is estimated empirically using eq 1. The 6-311G(d,p) basis set was employed.

hydrogen bond and the local electronic kinetic energy at the H···O BCP, G_b:[22c]

$$E_{int} = 0.429G_b \text{ (in atomic units)} \quad (5)$$

Equation 5 yields reasonable E_{int} values for molecular crystals with hydrogen bonding energy below ~85 kJ/mol.[13c]

We have applied eqs 4 and 5 to estimate the interaction energy for intermolecular C−H···O contacts and π-stacking interactions. The empirical relation eq 3 was also used to obtain the approximate energy of the intramolecular hydrogen bond in crystalline PANO. The results are given in Tables 2, 3, and 4.

4. RESULTS

PANO is known to crystallize in the monoclinic space group $P2_1/m$ with two molecules in the unit cell ($Z = 2$, $Z' = 0.5$), all molecules lying on the crystallographic mirror plane. The molecules form planar sheets {010} via C−H···O bonds (intrasheet contacts; see Figure 1a). Molecules of neighboring sheets bind to each other through π-stacking interactions (intersheet contacts, see Figure 1b), according to Desiraju.[39] Our experimental unit cell parameters (Table 1) and the bond distances (Tables 2−4) are in good agreement with the X-ray diffraction results obtained previously by Steiner et al. at 125 K.[40] The bond lengths of the optimized crystal structure derived from the solid state calculations do not differ significantly from the X-ray data. The details are reported in Supporting Information.

4.1. The Pattern of Noncovalent Interactions Based on Experimental and Theoretical Electron Densities. The QTAIMC analysis reveals that the basic molecule is linked in a crystal with 12 other molecules belonging to both the same layer and neighboring layers. Six molecules forming the planar

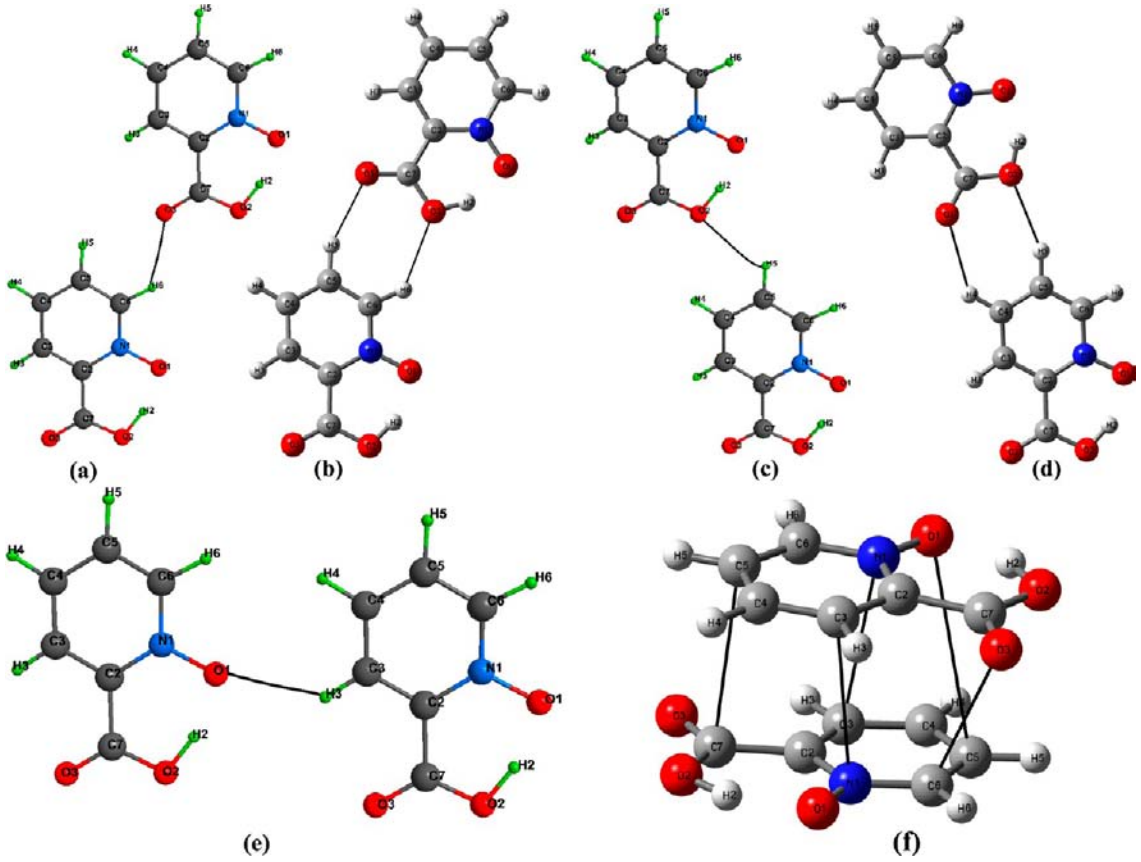

Figure 4. (a) The structure of an experimental crystalline fragment showing an intrasheet **C6−H6···O3** interaction; (b) the structure of an intrasheet H-bonded relaxed (B3LYP-D/6-311G(d,p)) ***intra_1*** model dimer; (c) the structure of an experimental crystalline fragment showing an intrasheet **C5−H5···O2** interaction; (d) the structure of an intrasheet H-bonded relaxed (B3LYP-D/6-311G(d,p)) ***intra_2*** model dimer; (e) the structure of an experimental crystalline fragment showing an intrasheet **C3−H3···O1** interaction; (f) the structure of a relaxed (B3LYP-D/6-311G(d,p)) ***intra_3*** intrasheet H-bonded model dimer. The black lines show the intermolecular bond paths.

dx.doi.org/10.1021/cg3015223 | Cryst. Growth Des. 2013, 13, 816−828

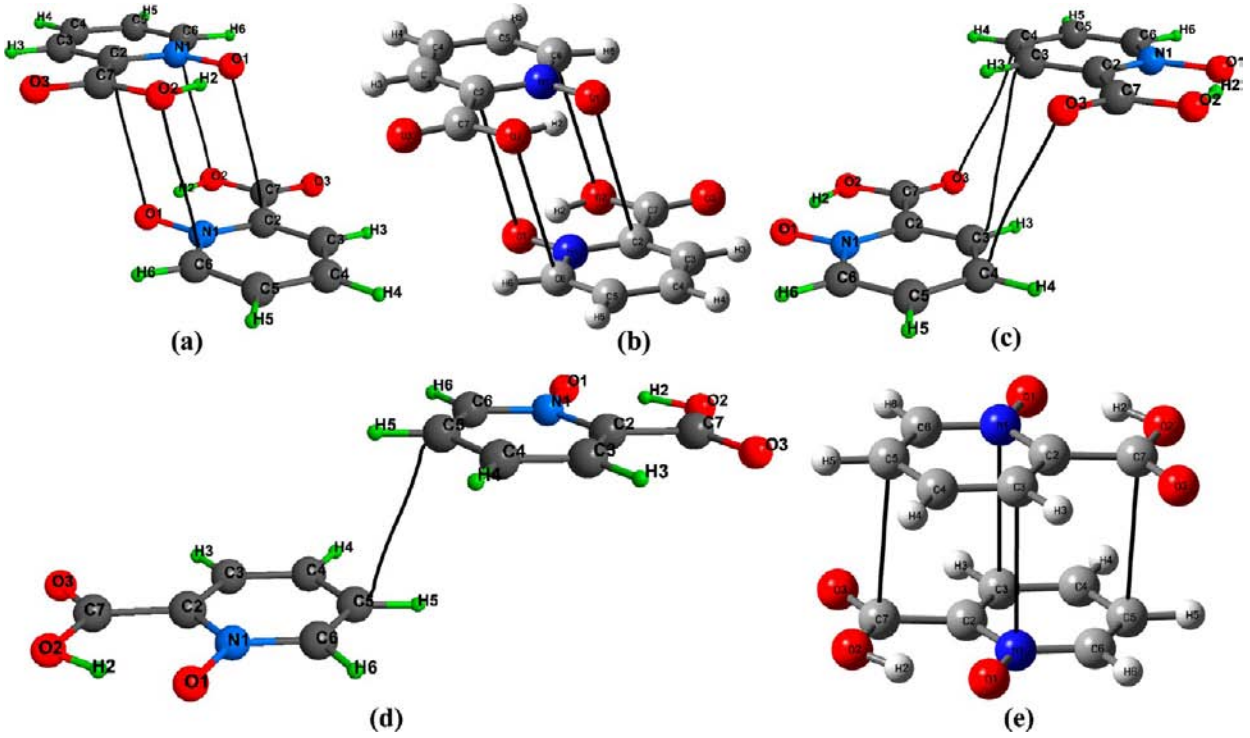

Figure 5. (a) The structure of an experimental crystalline pairwise stacked fragment **1**; (b) the structure of an intrasheet H-bonded relaxed (B3LYP-D/6-311G(d,p)) **inter_1** π-stacked model dimer; (c) the structure of an experimental crystalline pairwise stacked fragment **2**; (d) the structure of an experimental crystalline pairwise stacked fragment **3**; (e) the structure of a relaxed (B3LYP-D/6-311G(d,p)) **inter_4** intersheet π-stacked model dimer (it only exists in the gas phase). The black lines show the intermolecular bond paths.

sheet {010} are linked to the basic molecule by means of several types of intrasheet hydrogen bonds with distances varying between 2.3 and 2.6 Å (Table 2, Figure 4a,c,e). The experimental electron density shows three types of C−H···O intermolecular bond paths exhibiting $\nabla^2\rho(\mathbf{r}_b) > 0$ at the BCPs and electronic energy density $h_e(\mathbf{r}_b) > 0$ (Table 2). This is typical for closed shell interactions.[16j]

According to Gatti et al. (see Table 1 in ref 41), the energy of the C−H···O hydrogen bond estimated by eq 4 is less than 2 kJ/mol when the distance R(H···O) > 2.7 ± 0.1 Å. Such a bond is also characterized by a BCP electron density value less than 0.004 a.u., which is too small to be determined with certainty by the existing experimental and theoretical methods.[42] Therefore, we will further discuss only the intrasheet C−H···O contacts in the PANO crystal with R(H···O) < 2.7 ± 0.1 Å. The intrasheet C−H···O interaction energy values, evaluated according to eq 4 and 5, show that the C6−H6···O3 interaction is the strongest one (Table 2, Figure 4a).

Molecular sheets {010} lie in planes perpendicular to the b axis of the unit cell with an intersheet distance of 3.017 Å. QTAIMC analysis reveals that these sheets are linked by means of five different types of π-stacking contacts (Figures 1b and 5a,c,d). The electron density features of the π-stacking BCPs are given in Table 3. We note that these features are relatively small ($\rho_b \sim 0.006(1)$ a.u.) and are comparable to the experimental noise in the reconstructed electron density. Therefore, to establish whether the experimental electron density, $\rho(\mathbf{r})$, along the π-stacking contacts carries any bonding information, we have analyzed it in these regions in terms of information theory.[43] The Shannon[44] information entropy density is defined in terms of $\rho(\mathbf{r})$ as[45]

$$s(\mathbf{r}) = -\frac{\rho(\mathbf{r})}{N} \ln \frac{\rho(\mathbf{r})}{N} \tag{6}$$

where N is the number of electrons in a unit cell. This function evaluates (in a statistical sense) the structural order, or lack thereof, in the continuous spatial distribution of electrons. The constructive interference of atomic valence orbitals along the bond paths forms the electron accumulation regions. The electron correlation in these regions tends to raise the entropy density due to an additional lack of information about electron positions in space relative to the density of the unbound state.[46] Thus, the entropy density is able to measure the electron localization/delocalization in direct (position) space. For the π-stacking contacts, it is reasonable to compare the entropy density $s_b(\mathbf{r})$ corresponding to the experimental $\rho(\mathbf{r})$ at the BCPs with the entropy density of the experimental electron density noise, $s_{noise}(\mathbf{r})$, i.e., entropy density of a uniform electron distribution, whose values are equal to the statistical electron-density errors at the same points. Shannon entropy density maps for some π-stacking contacts in PANO are shown in Figure 6, together with the local entropy density values, $s_b(\mathbf{r})$ and $s_{noise}(\mathbf{r})$ at the BCPs (note that noise is uniform around the BCPs whereas $s_{noise}(\mathbf{r})$ is constant). These results show that the "experimental" entropy density values at the π-stacking BCPs significantly exceed the experimental noise entropy $s_{noise}(\mathbf{r})$. This leads to the conclusion that the experimental electron density indeed carries information on the electron density accumulation along the π-stacking contacts in PANO. Thus the discussion of the effects resulting from intermolecular π-stacking is physically grounded.

There are three types of pairwise stacked molecules in the crystal (Figure 5a,c,d). In fragment **1**, molecules are arranged one above the other with "head-to-tail" orientation, and the

dx.doi.org/10.1021/cg3015223 | Cryst. Growth Des. 2013, 13, 816−828

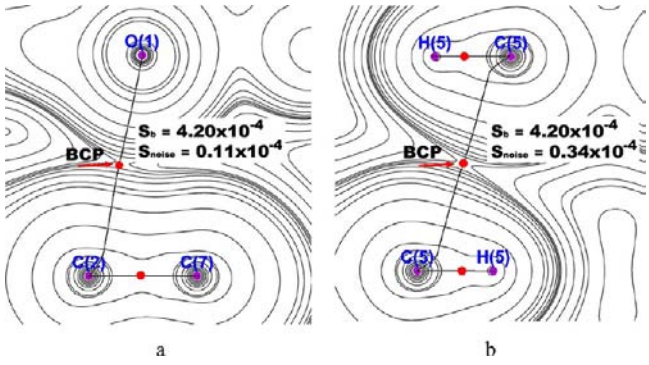

Figure 6. Shannon entropy density maps including some π-stacking contacts in the PANO crystal. The BCPs (3,−1) in the electron density are shown by the red points.

centers of gravity of the cyclic hydrogen bonded moieties of the molecules (O1−N1−C2−C7−O2−H2) aligned parallel to the *b* axis of the unit cell (Figure 5a). In fragment **2**, molecules in adjacent sheets are shifted relative to each other parallel to the *a* axis (Figure 5c). In fragment **3**, the pyrimidine rings of nearby molecules face each other and are shifted relative to each other parallel to the *c* axis (Figure 5d). In contrast to urea, a benchmark molecular crystal with relatively weak N−H···O bonds, E_{int} < 20 kJ/mol,[19a,15a] no strong specific structure-forming intermolecular interactions exist in crystalline PANO.

The energies of the particular noncovalent interactions in the PANO crystal derived from electron density parameters at the corresponding bond critical points using the empirical schemes eqs 4 and 5 are given in Tables 2, 3, and S5. We note that application of eqs 4 and 5 for estimating the π-stacking energy[19b,47] needs justification because the parameters in 4 and 5 were obtained for hydrogen bonds only. The interlayer interaction energy ΔE_{layer} has been calculated as the difference between the total energy of two molecular {010} layers and double the energy of a single layer. The resulting value was corrected for basis set superposition error. ΔE_{layer} can be considered as the total interaction energy of intersheet π-stacking contacts. The computation is straightforward[48] with the program CRYSTAL09 (see Supporting Information) and leads to a π-stacking interaction energy of ∼61 kJ/mol. Corresponding values estimated by eqs 4 and 5 are 55.2 and 61.9 kJ/mol, respectively (Table 6). We can thus conclude that eq 5 gives reasonable values for the π-stacking interaction energy in this case.

The energies of intramolecular O−H···O interactions calculated by eq 3 are given in Table 4. E_{int} reaches 107.9 kJ/mol in the case of the experimental geometrical parameters and varies from 88 to 103 kJ/mol for periodic models.

Thus, the PANO crystal packing is influenced by the interplay of three types of noncovalent interactions of different strength and nature. The strong intramolecular O1−H1···O2 hydrogen bond (E_{int} > 90 kJ/mol) aids in the formation of an additional planar "six-membered ring" in the molecular structure. The intrasheet packing of the molecules is mainly determined by the general shape of the molecules and the existence of weak C−H···O hydrogen bonds (E_{int} < 10 kJ/mol) which form layers. The mutual orientation of molecules in adjacent sheets are mainly caused by the weak π-stacking interactions (E_{int} < 4 kJ/mol).

DFT computations with the Grimme correction for the dispersion energy have been successfully applied for the description of weak intermolecular interactions (E_{int} < 10 kJ/mol) in molecular crystals.[5,16i,49] To the best of our knowledge, crystals with noncovalent interactions of different strength, such as observed in the PANO crystal, were not yet studied using the Grimme dispersion correction. Selected geometrical parameters of the PANO crystal as well as periodic electron density features obtained with and without the Grimme dispersion correction are given in Tables 2, 4, and S5. We should

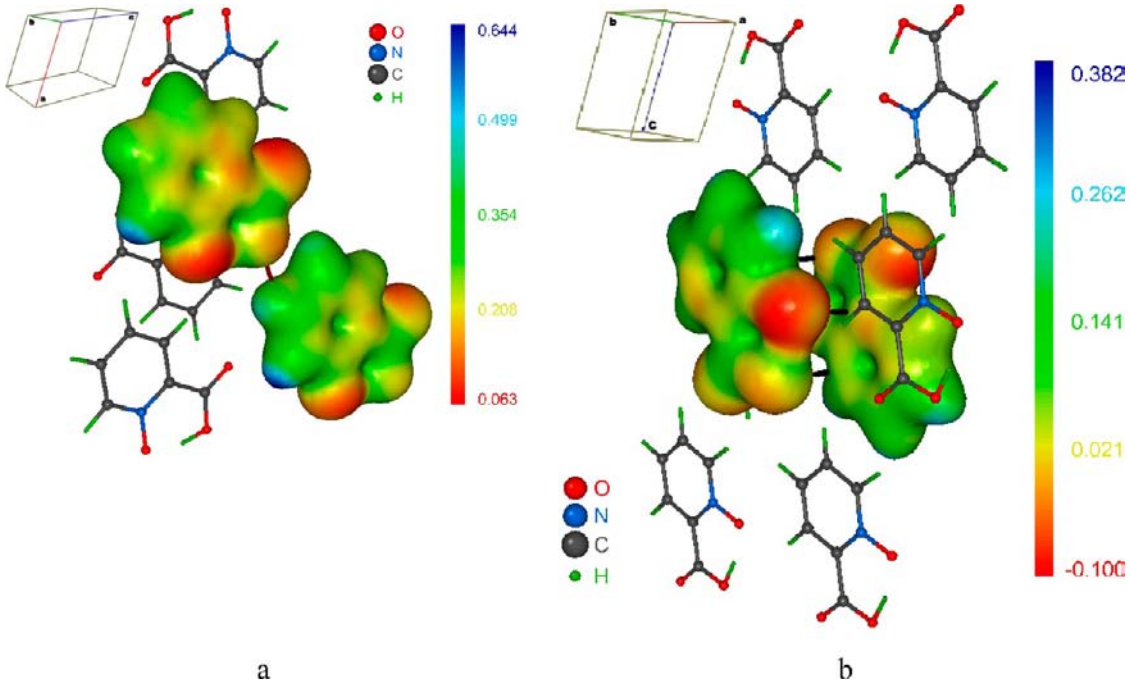

Figure 7. The experimental electrostatic potential in the PANO crystal projected onto the 3D-isosurfaces of the experimental electron density (0.016 a.u.) together with the intermolecular H-bond (a) and π-stacking (b) bond paths.

dx.doi.org/10.1021/cg3015223 | *Cryst. Growth Des.* 2013, 13, 816−828

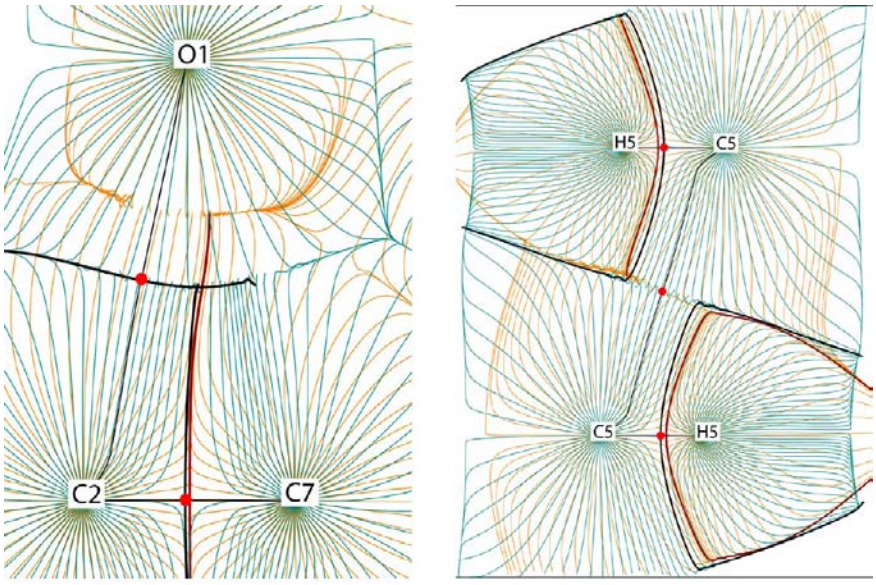

Figure 8. The superposition of gradient fields in the experimental electron density (blue) and the electrostatic potential (orange) in the planes containing intermolecular C···O (a) and C5···C5 (b) bond paths (thin black lines). The bold lines correspond to the zero-flux atomic boundaries. The critical points (3,−1) in the electron density are shown by the red points.

remember that this correction is empirical and changes the crystal wave function in an indirect way through the change in the atomic positions. Table 2 shows that the H···O distances of the C−H···O intrasheet contacts computed with the Grimme dispersion correction are in better agreement with experimental values. The same results are obtained for the electron density features of these contacts. On the other hand, the Grimme dispersion correction leads to a significant change in the geometrical and QTAIMC parameters of the strong intramolecular O−H···O bond (Tables 2 and 4). The correction worsens the agreement with the experimental intramolecular O···O distance, elongating it by ∼0.02 Å. Note that this effect does not depend on the type of the DFT functional (Table S5). Concomitantly, the OH-stretching vibration frequency increases by more than 100 cm^{-1} (Table 4).

Thus, for the PANO crystal, the Grimme dispersion correction improves the agreement of the computed geometrical and QTAIMC characteristics of the intermolecular contacts with experimental values but worsens the agreement between parameters for the strong short intramolecular O−H···O bond. We may speculate that the Grimme dispersion correction should be used with caution for simultaneous description of both weak and strong noncovalent interactions in molecular crystals.

4.2. The Electrostatic Potential Features of the Noncovalent Interactions. We now consider the features of the electrostatic interactions in crystalline PANO in terms of the electrostatic potential (ESP), $\varphi(\mathbf{r})$, derived from the experimental electron density plus the nuclear contribution. Figure 7 shows the ESP mapped onto the 0.016 a.u. isodensity surface. The ESP in a crystal is a continuous well-structured function,[50] and Figure 7 illustrates the correspondence between bond paths in the electron density and the ESP values along these bond paths.[51] The electrostatic interaction does not exhibit directional character. Indeed, the vector $\nabla\varphi(\mathbf{r})$, i.e., the inner-crystal electrostatic force $\mathbf{F}(\mathbf{r}) = -\nabla\varphi(\mathbf{r})$ changes its sign at the (3,−1) BCP point in the φ-field; therefore, the electrostatic force originating in one atomic basin delimited by the zero-flux condition, $\nabla\varphi(\mathbf{r})\cdot\mathbf{n}(\mathbf{r}) = 0$, and ending in another such basin does not exist. At the same time, the bond paths in the electron density corresponding to C···O π-stacking contacts and hydrogen bonds pass through slightly different ESP values on the 0.016 a.u. surfaces in adjacent molecules. This reflects the electrostatic complementarity of corresponding moieties when they are at some distance from each other. The gradient of the ESP along the bond paths corresponding to C···C π-stacking contacts is nearly zero, and the above-mentioned complementarity is not observed.

To clarify the nature of these interactions, we remember that the electron density within each φ-basin is attracted to the corresponding nucleus. Considering the superposition of the ρ-basins and φ-basins of adjacent atoms A and B of different kind,[15i,51,52] we note that the part of the electron density belonging to atom A falls into the φ-basin of atom B. Thus, along the C···O π-stacking contacts (Figure 8), the ρ-basin of the C atom overlaps the φ-basin of the O atom of the neighboring molecule. Such picture is also observed for all the hydrogen bonds. At the same time, the boundaries of the ρ-basins and φ-basins of atoms of the same kind, such as C5 and C5′ (Figure 8) as well as C3 and C3′, which are linked by the bond paths forming the C···C π-stacking contacts, coincide in the given planes. Thus the C···C π-stacking contacts in a PANO crystal are mainly due to electrostatic attraction of the electrons in the bonded atoms to their "own" nuclei plus the dispersion interaction.

4.3. The Energetic Features of Crystalline PANO. To check the accuracy of the energies of the C−H···O hydrogen bonds and π-stacking interactions determined from electron-density parameters, eqs 4 and 5, we have evaluated E'_{latt} (see eq 2 and Supporting Information) and compared its value with the experimental sublimation energy reduced to 0 K[53] and the theoretical E_{latt} value calculated using an *ab initio* approach; see eq 1. Obtained results are given in Table 6. Two different schemes to evaluate the noncovalent energy (see eqs 4 and 5),

dx.doi.org/10.1021/cg3015223 | *Cryst. Growth Des.* 2013, 13, 816−828

lead to a lattice energy of 92.9 and 116.1 kJ/mol, respectively. These numbers are in good agreement with both the experimental sublimation energy (98.9 kJ/mol) and the *ab initio* lattice energy corrected for basis set superposition error[54] (115 kJ/mol). We conclude that the electron-density based approach to noncovalent interaction energy evaluation gives reasonable values for lattice energies.

5. DISCUSSION

The cluster approximation is widely used for the description of noncovalent interactions. A particular intermolecular interaction is modeled using a molecular synthon, the structure of which is extracted from a corresponding crystal. This approximation is often used to model supramolecular systems/crystals, whose stability is determined by hydrogen bonds of different strengths and π-stacking interactions.[19c−g,55,56,15i] However, the applicability of the cluster approximation for the description of noncovalent interactions in a crystal is vague; the use of even relatively large molecular clusters (tetramers, pentamers, hexamers, etc.) still provides an insufficient description of the effects of the crystalline environment.[17c,16g,57] To clarify the reason for that, let us discuss the applicability of the cluster approximation in its simplest and often used form, where isolated (i.e., gas phase) molecular dimers are considered.[57]

5.1. Intersheet π-Stacking Contacts. The cofacial conformation with parallel molecular planes corresponds to a global/local minimum on the dimer potential energy surface if the interacting molecules have a dipole moment. Such cofacial dimers are often studied by taking two adjacent molecules from a crystal structure[19j,k] for which single-point computations are then performed (a "frozen dimer" model).[19g,j,k,o] It may differ significantly from that corresponding to the potential energy surface minimum (optimized) for a gas-phase dimer/cluster.[58] Remembering that QTAIMC in its current form is designed for the equilibrium state, the description of the interactions in such a dimer in terms of the BCP features has no physical meaning.[14d] Moreover, the difference between the two mentioned geometries can be so significant that the interaction pattern between a pair of molecules is completely changed. Unfortunately we cannot anticipate how large this difference will be for each specific case. To illustrate this point, taking PANO as an example, three types of dimers were considered (Figure 5a,c,d). Frequency analysis (B3LYP-D/6-311G (d,p)) shows that all three "frozen-dimer" structures do not correspond to local minima on the gas-phase potential energy surface. Subsequent optimization of geometry preserves the parallel planarity of the dimers, but the distance between the planes is reduced by ∼0.17 Å (**inter_1**) and ∼0.16 Å (**inter_2** and **inter_3**). The structures obtained by this procedure will be called "relaxed" dimers. The set of noncovalent intermolecular interactions in the relaxed **inter_1** dimer (Table 5, Figure 5b) is the same as the one in the frozen dimer. After the geometry optimization, the values of the electron density at the BCPs change insignificantly (Table 5), despite the bond lengths being reduced by 0.191 Å (C2···O1) and 0.156 Å (C6···O2). The *ab initio* energy of the π-stacking interactions is 28 kJ/mol (taking into account basis set superposition error and zero-point energy corrections) and agrees with estimates based on electron density features (Table 5).

As a result of geometry optimization, in contrast to **inter_1** the pattern of noncovalent interactions in **inter_2** and **inter_3** dimers collapses to form a stable **inter_4** dimer. This

Table 5. Selected Geometrical and Electron Density Characteristics (a.u.) of the Intersheet π-Stacking Interactions for the Frozen Dimer/B3LYP-D/6-311G(d,p) Extracted from the Crystal Structure, inter_1 Optimized Dimer/B3LYP-D/6-311G(d,p), the Fragment from the Optimized Crystal Unit Cell B3LYP-D/6-311G(d,p), the Fragment from the Experimental Crystal Unit Cell[a]

method	contact	R, Å	$\rho(r)$	$\nabla^2\rho(r)$	E_{int},[b] kJ/mol	E_{total},[c] kJ/mol
frozen dimer	C2···O1	3.216	0.006	0.022	5.2	21
	C6···O2	3.185	0.006	0.022	5.2	
optimized dimer	C2···O1	3.025	0.009	0.031	7.9	29
	C6···O2	3.029	0.008	0.028	6.6	
optimized crystal	C2···O1	3.234	0.006	0.022	3.9	16
	C6···O2	3.202	0.006	0.024	3.9	
experiment	C2···O1	3.209	0.006	0.023	3.9	16
	C6···O2	3.179	0.006	0.024	3.9	

[a]B3LYP-D stands for B3LYP with the Grimme dispersion correction. [b]E_{int} is the energy of the contact evaluated with eq 4. [c]The value is obtained by the summing of E_{int} for all C2···O1 and C6···O2 interactions corresponding to the binding energy of synthon.

Table 6. The Lattice Energy (kJ/mol) of Crystalline PANO Evaluated Using Different Approaches[a]

	decomposition of the E_{latt}		
approach	H-bonds	Pi-stacking	lattice energy
eq 2, V_b[b]	48.1	44.8	92.9
eq 2, G_b[c]	54.2	61.9	116.1
eq 1		61.0[d]	115.0
ΔH°_{sub}[e]			98.9

[a]Decomposition of the E_{latt} into the total H-bonded and π-stacking energies is also given, where it is possible. [b]The energies computed using the electronic potential energy density, V_b, at the bond critical point; see eq 4. [c]The energies computed using the electronic kinetic energy density, G_b, at the bond critical point; see eq 5. [d]SLAB model, see Supporting Information. [e]Sublimation energy reduced to 0 K; see ref 53.

corresponds to a local minimum on the gas-phase potential energy surface, but does not exist in the α-form of crystalline PANO (Tables S6−S8, Figure 5e). The cofacial conformation of the **inter_4** dimer is stabilized by N1···C3 and C7···C5 π-stacking interactions, while the C4···O3, C3···C3 and C5···C5 interactions are responsible for stabilization in **inter_2** (Table S6) and **inter_3** (Table S7) frozen dimers. Taking into account basis set superposition error and zero-point energy, the total energy of π-stacking interactions in the **inter_4** dimer is 39 kJ/mol.

The comparison of the computed characteristics in the relaxed and frozen dimers allows us to distinguish two limiting cases of the influence of the crystal environment on the π-stacking interactions in dimers with a cofacial conformation. In the first case, the mutual orientation of the molecules is practically the same. This allows an immediate transfer of the electron density characteristics, derived for the cluster approximation, to the crystal. In the second case, the dimer structure is strongly distorted, and the resulting set of π-stacking interactions has no relation to the crystal. In this case, the transfer of the gas-phase characteristics to the crystal (and vice versa) is inappropriate.

dx.doi.org/10.1021/cg3015223 | Cryst. Growth Des. 2013, 13, 816−828

5.2. C−H···O Intrasheet Contacts. For intrasheet hydrogen bonds in PANO, three types of frozen dimers were introduced (see above subsection 4.1) (Figure 4a,c,e), but none corresponds to a local minimum on the gas-phase potential energy surface. Moreover, geometry optimization leads to a strong distortion of the mutual orientation of the molecules in these dimers. In the cases of the ***intra_1*** and ***intra_2*** dimers, the pattern of intermolecular C−H···O contacts is changed (Figure 4a−d). In each of the frozen dimers, as well as in each crystal fragment, only a single hydrogen bond to an adjacent molecule is formed. At the same time, geometry optimization results in the formation of another hydrogen bond pattern in each of the pieces. Correspondingly, the spectral and QTAIMC characteristics of both ***intra_1*** and ***intra_2*** dimers are changed (Tables 4, S9 and S10).

Geometry optimization strongly changes the mutual orientation of the molecules in the ***intra_3*** dimer as well (Figure 4e,f, Table S11): essentially, a new dimer is formed. It is stabilized by a set of π-stacking interactions and its structure resembles the one of the intersheet dimer, **inter_4**. Thus, the optimized gas-phase characteristics in PANO are not transferrable to a crystal for these dimers either.

5.3. Intramolecular Hydrogen Bonds. The effects of the crystalline environment on the structural and spectroscopic properties of the intramolecular hydrogen bond in PANO are presented in Table 4. The geometrical and spectroscopic parameters obtained from the 3D periodic model are in good agreement with experimental data. In the cluster approximation, the O···O distance is much longer than the experimental value, and, therefore, the computed frequency of the OH stretching vibration is too high compared to the experimental and 3D periodic values. Similar results were obtained previously.[17c]

6. CONCLUSIONS

The pattern of noncovalent interactions in the picolinic acid N-oxide crystal has been identified and quantified using the electron density features derived from high resolution X-ray diffraction data collected at 100 K and periodic DFT calculations with the Grimme dispersion correction. The present study shows that any strong specific intermolecular interactions are absent in crystalline picolinic acid N-oxide. The crystal packing is influenced by the interplay of three types of noncovalent interactions of different strength and nature. The strong intramolecular O−H···O hydrogen bond (E_{int} > 90 kJ/mol) completes a six-membered ring in the molecular structure. The intrasheet interactions in the crystal are mainly determined by the weak C−H···O hydrogen bonds (E_{int} < 10 kJ/mol). The mutual orientation of molecules in adjacent sheets is derived from the weak π-stacking interactions, whose energy (E_{int} < 4 kJ/mol) may be evaluated using the empirical correlation between E_{int} and the electron density parameters at the corresponding bond critical points. The determined features of these weak interactions are indeed significant, as demonstrated using information theory.

The empirical Grimme dispersion correction improves the agreement between the computed and experimental geometrical and topological electron-density characteristics of the intermolecular contacts in the PANO crystal. At the same time, it worsens the agreement of the geometrical and spectral parameters for the strong short intramolecular O−H···O bond. It can be concluded that the Grimme dispersion correction does not provide an adequate simultaneous description of weak and strong noncovalent interactions in the PANO crystal.

The superposition of the gradient fields in the electron density and electrostatic potential helps to understand the pattern of nondirectional electrostatic interactions in the PANO crystal in terms of QTAIMC. This picture can be considered as a result of the partial overlap of neighboring atomic basins in the electron density and zero-flux basins in the electrostatic potential. The physical mechanism of the electrostatic interactions is the same both for intramolecular shared-shell interactions (including the O−H···O hydrogen bond), intermolecular C−H···O hydrogen bonds and π-stacking closed-shell interactions. The aforementioned overlap in the π-stacking contacts in a PANO crystal is very small; therefore, the electrostatic contribution to the π-stacking interaction consists mainly of the classic attraction of electrons in the deformed bonded atoms to their "own" nuclei.

Cluster models should be used for the description of a particular type of noncovalent interaction in crystals with caution. This model can be applied if the mutual orientation of the molecules in a cluster is maintained after geometry optimization, compared to that in the crystal.

In the present study we applied an approach for noncovalent interaction energy evaluation from the electron density parameters. It enables one to estimate the lattice energy of the considered crystals as the total intermolecular interaction energy. The value obtained for the lattice energy is in reasonable agreement with both the experimental sublimation energy and the *ab initio* lattice energy.

■ ASSOCIATED CONTENT

Ⓢ Supporting Information

Crystallographic information file (CIF) for studied compound, the residual experimental Fourier electron-density maps, complete tables of BCP properties obtained from experiment and computations for all covalent bonds and noncovalent interactions, the electron-density features of the intramolecular hydrogen bond, the details of determination of interaction energy. This material is available free of charge via the Internet at http://pubs.acs.org.

■ AUTHOR INFORMATION

Corresponding Author

*E-mail: vtsirelson@yandex.ru.

Notes

The authors declare no competing financial interest.

■ ACKNOWLEDGMENTS

This study is supported by the Russian Ministry for Education and Science and the Russian Foundation for Basic Research (Grants 10-03-00611 and 11-03-00583). A.A.P. thanks the National Science Foundation for partial support of this work (Grant NSF-CHE-1213329).

■ REFERENCES

(1) Buckingham, A. D. In *Crystal Engineering: The Design and Application of Functional Solids*; Seddon, K. R., Zaworotko, M., Eds. NATO Science Series C, Vol. 539; Kluwer Academic: Boston, 1999; pp 49−68.

(2) (a) Fogassy, E.; Nogradi, M.; Kozma, D.; Egri, G.; Palovics, E.; Kiss, V. *Org. Biomol. Chem.* **2006**, *4*, 3011−3030. (b) Karamertzanis, P. G.; Anandamanoharan, P. R.; Fernandes, P.; Cains, P. W.; Vickers, M.; Tocher, D. A.; Florence, A. J.; Price, S. L. *J. Phys. Chem. B* **2007**, *111*,

5326−5336. (c) Gourlay, M. D.; Kendrick, J.; Leusen, F. J. J. *Cryst. Growth Des.* **2007**, *7*, 56. (d) Price, S. L. *Adv. Drug Delivery Rev.* **2004**, *56*, 301−309.
(3) (a) Evans, O. R.; Lin, W. B. *Acc. Chem. Res.* **2002**, *35*, 511−522. (b) Roesky, H. W.; Andruh, M. *Coord. Chem. Rev.* **2003**, *236*, 91−119. (c) Kwon, O.-P.; Ruiz, B.; Choubye, A.; Mutter, L.; Schneider, A.; Jazbinesek, M.; Gramlich, V.; Gunter, P. *Chem. Mater.* **2006**, *18*, 4049−4054.
(4) (a) Malaspina, L.; Gigli, R.; Bardi, G. *J. Chem. Phys.* **1973**, *59*, 387−394. (b) Murata, S.; Sakiyama, M.; Seki, S. *J. Chem. Thermodynamics* **1982**, *14*, 707−721. (c) Sabbah, R.; Antipine, I.; Coten, M.; Davy, L. *Thermochim. Acta* **1987**, *115*, 153−165. (d) Holdiness, M. R. *Thermochim. Acta* **1983**, *68*, 375−377.
(5) Civalleri, B.; Zicovich-Wilson, C. M.; Valenzano, L.; Ugliengo, P. *CrystEngComm* **2008**, *10*, 405−410.
(6) Maschio, L.; Civalleri, B.; Ugliengo, P.; Gavezzotti, A. *J. Phys. Chem. A* **2011**, *115*, 11179−11186.
(7) (a) Dominiak, P. M.; Espinosa, E.; Angyan, J. In *Intermolecular Interactions Energies from Experimental Charge Density Studies from Charge Density Studies in Modern Charge Density Analysis*; Gatti, C., Macchi, P., Eds.; Springer: Heidelberg, London, NY, 2012; pp 387−433. (b) Civalleri, B.; Doll, K.; Zicovich-Wilson, C. M. *J. Phys. Chem. B* **2007**, *111*, 26−33.
(8) (a) Ouvrard, C.; Mitchell, J. B. O. *Acta Crystallogr. B* **2003**, *59*, 676−685. (b) Day, G. M. *Crystallogr. Rev.* **2011**, *17*, 3−52 and references therein. (c) Pertsin, A. J.; Kitaigorodsky, A. I. *The Atom-Atom Potential Method. Application to Organic Molecular Solids*; Springer-Verlag: New York, 1987. (d) Price, S. L. *Acc. Chem. Res.* **2009**, *42*, 117−126. (e) Lommerse, J. P. M.; Motherwell, W. D. S.; Ammon, H. L.; Dunitz, J. D.; Gavezzotti, A.; Hofmann, D.W. M.; Leusen, F. J. J.; Mooij, W. T. M.; Price, S. L.; Schweizer, B.; Schmidt, M. U.; van Eijck, B. P.; Verwer, P.; Williams, D. E. *Acta Crystallogr., Sect. B* **2000**, *56*, 697−714. (f) Motherwell, W. D. S.; Ammon, H. L.; Dunitz, J. D.; Dzyabchenko, A.; Erk, P.; Gavezzotti, A.; Hofmann, D. W. M.; Leusen, F. J. J.; Lommerse, J. P. M.; Mooij, W. T. M.; Price, S. L.; Scheraga, H.; Schweizer, B.; Schmidt, M. U.; van Eijck, B. P.; Verwer, P.; Williams, D. E. *Acta Crystallogr., Sect. B* **2002**, *58*, 647−661. (g) Dunitz, J. D.; Gavezzotti, A. *Angew. Chem., Int. Ed.* **2005**, *44*, 1766−1787.
(9) Sancho-García, J. C.; Olivier, Y. *J. Chem. Phys.* **2012**, *137*, 194311.
(10) Dzyabchenko, A.; Scheraga, H. A. *Acta Crystallogr., Sect. B* **2004**, *60*, 228−237.
(11) Dunitz, J. D.; Gavezzotti, A. *Chem. Soc. Rev.* **2009**, *38*, 2622−2633.
(12) (a) Bader, R. F. W. *Atoms in Molecules - A Quantum Theory*; Oxford University Press: Oxford, 1990. (b) Tsirelson, V. G. In *The Quantum Theory of Atoms in Molecules: From Solid State to DNA and Drug Design*; Matta, C., Boyd, R., Eds.; Wiley-VCH: New York, 2007; Chapter 10.
(13) (a) Nelyubina, Y. V.; Antipin, M. Yu.; Lyssenko, K. A. *J. Phys. Chem. A* **2007**, *111*, 1091−1095. (b) Nelyubina, Y. V.; Antipin, M. Yu.; Cherepanov, I. A.; Lyssenko, K. A. *CrystEngComm* **2010**, *12*, 77−81. (c) Vener, M. V.; Egorova, A. N.; Churakov, A. V; Tsirelson, V. G. *J. Comput. Chem.* **2012**, *33*, 2303−2309.
(14) (a) Desiraju, G. R. *Crystal Design: Structure and Function Perspectives in Supramolecular Chemistry*; Desiraju, G. R., Ed.; Chichester: Wiley, 2003; *Vol. 7*. (b) Brock, C. P.; Dunitz, J. D. *Chem. Mater.* **1994**, *6*, 1118−1127. (c) Sekhon, B. S. *Ars Pharm.* **2009**, *50*, 99−117. (d) Price, S. L. *Acc. Chem. Res.* **2009**, *42*, 117−126. (e) Berkovitch-Yellin, Z.; Leiserowitz, L. *Acta Crystallogr., Sect. B* **1984**, *40*, 159−165.
(15) (a) Suponitsky, K. Y.; Tsirelson, V. G.; Feil, D. *Acta Crystallogr., Sect. A* **1999**, *55*, 821−827. (b) Morrison, C. A.; Siddick, M. M. *Chem.—Eur. J.* **2003**, *9*, 628−634. (c) Vishweshwar, P.; Babu, N. J.; Nangia, A.; Mason, S. A.; Puschmann, H.; Mondal, R.; Howard, J. A. K. *J. Phys. Chem. A* **2004**, *108*, 9406−9416. (d) Schmidtmann, M.; Farrugia, L. J.; Middlemiss, D. S.; Gutmann, M. J.; McIntyre, G. J.; Wilson, C. C. *J. Phys. Chem. A* **2009**, *113*, 13985−13997. (e) Dittrich, B.; Weber, M.; Kalinowski, R.; Grabowsky, S.; Hubschle, C. B.; Luger, P. *Acta Crystallogr., Sect. B* **2009**, *65*, 749−756. (f) Hathwar, V. R.; Guru Row, T. N. *Cryst. Growth Des.* **2011**, *11*, 1338−1346. (g) Hathwar, V. R.; Thakur, T. S.; Dubey, R.; Pavan, M. S.; Guru Row, T. N.; Desiraju, G. R. *J. Phys. Chem. A* **2011**, *115*, 12852−12863. (h) Hathwar, V. R.; Gonnade, R. G.; Munshi, P.; Bhadbhade, M. M.; Guru Row, T. N. *Cryst. Growth Des.* **2011**, *11*, 1855−1862. (i) Krawczuk, A.; Stadnicka, K. *J. Phys. Chem. A* **2012**, *116*, 9759−9768.
(16) (a) Platts, J. A.; Howard, S. T. *J. Chem. Phys.* **1996**, *105*, 4668−4674. (b) Vener, M. V.; Manaev, A. V.; Egorova, A. N.; Tsirelson, V. G. *J. Phys. Chem. A* **2007**, *111*, 1155−1162. (c) Bertini, L.; Cargnoni, F.; Gatti, C. *Theor. Chem. Acc.* **2007**, *117*, 847−884. (d) Gibbs, G. V.; Downs, R. T.; Cox, D. F.; Ross, N. L.; Boisen, M. B.; Rosso, K. M. *J. Phys. Chem. A* **2008**, *112*, 3693−3699. (e) Presti, L. L.; Ellern, A.; Destro, R.; Lunelli, B. *J. Phys. Chem. A* **2009**, *113*, 3186−3196. (f) Vener, M. V.; Egorova, A. N.; Tsirelson, V. G. *Chem. Phys. Lett.* **2010**, *500*, 272−276. (g) Götz, K.; Meier, F.; Gatti, C.; Burow, A. M.; Sierka, M.; Sauer, J.; Kaupp, M. *J. Comput. Chem.* **2010**, *31*, 2568−2576. (h) Churakov, A. V.; Prikhodchenko, P. V.; Lev, O.; Medvedev, A. G.; Tripol'skaya, T. A.; Vener, M. V. *J. Chem. Phys.* **2010**, *133* (164506), 1−9. (i) Shishkina, A. V.; Stash, A. I.; Civalleri, B.; Ellern, A.; Tsirelson, V. G. *Mendeleev Commun.* **2010**, *20*, 161−164. (j) Vener, M. V.; Medvedev, A. G.; Churakov, A. V.; Prikhodchenko, P. V.; Tripol'skaya, T. A.; Lev, O. *J. Phys. Chem. A* **2011**, *115*, 13657−13663.
(17) (a) Stare, J.; Mavri, J.; Ambrožić, G.; Hadži, D. *J. Mol. Struct. (THEOCHEM)* **2000**, *500*, 429−440. (b) Stare, J.; Panek, J.; Eckert, J.; Grdadolnik, J.; Mavri, J.; Hadži, D. *J. Phys. Chem. A* **2008**, *112*, 1576−1586. (c) Panek, J.; Stare, J.; Hadzi, D. *J. Phys. Chem. A* **2004**, *108*, 7417−7423.
(18) (a) Grimme, S. *J. Comput. Chem.* **2006**, *27*, 1787−1799. (b) Von Lilienfeld, O. A.; Tkatchenko, A. *J. Chem. Phys.* **2010**, *132* (234109), 1−11. (c) Grimme, S.; Antony, J.; Schwabe, T.; Mück-Lichtenfeld, C. *Org. Biomol. Chem.* **2007**, *5*, 741−758.
(19) (a) Karamertzanis, H. G.; Day, G. M.; Welch, G. W. A.; Kendrick, J.; Leusen, F. J. J.; Neumann, M. A.; Price, S. L. *J. Chem. Phys.* **2008**, *128* (244708), 1−17. (b) Matta, C. F.; Castillo, N.; Boyd, R. J. *J. Phys. Chem. B* **2006**, *110*, 563−578. (c) Rutledge, L. R.; Wetmore, S. D. *J. Chem. Theory Comput.* **2008**, *4*, 1768−1780. (d) Rutledge, L. R.; Campbell-Verduyn, L. S.; Hunter, K. C.; Wetmore, S. D. *J. Phys. Chem. B* **2006**, *110*, 19652−19663. (e) Acosta-Silva, C.; Branchadell, V.; Bertran, J.; Oliva, A. *J. Phys. Chem. B* **2010**, *114*, 10217−10227. (f) González Moa, M. J.; Mandado, M.; Mosquera, R. A. *J. Phys. Chem. A* **2007**, *111*, 1998−2001. (g) Kamya, P. R. N.; Muchall, H. M. *J. Phys. Chem. A* **2011**, *115*, 12800−12808. (h) Estévez, L.; Otero, N.; Mosquera, R. A. *J. Phys. Chem. A* **2009**, *113*, 11051−11058. (i) Rutledge, L. R.; Navarro-Whyte, L.; Peterson, T. L.; Wetmore, S. D. *J. Phys. Chem. A* **2011**, *115*, 12646−12658. (j) Shishkin, O. V.; Dyakonenko, V. V.; Maleev, A. V.; Schollmeyer, D.; Vysotsky, M. O. *CrystEngComm* **2011**, *13*, 800−805. (k) Dyakonenko, V. V.; Maleev, A. V.; Zbruyev, A. I.; Chebanov, V. A.; Desenko, S. M.; Shishkin, O. V. *CrystEngComm* **2010**, *12*, 1816−1823. (l) Sarma, R. J.; Tamuly, C.; Barooah, N.; Baruah, J. B. *J. Mol. Struct.* **2007**, *829*, 29−36. (m) Reger, D. L.; Debreczeni, A.; Horger, J. J.; Smith, M. D. *Cryst. Growth Des.* **2011**, *11*, 4068−4079. (n) Wilsona, C. R.; Munroa, O. Q. *Acta Crystallogr., Sect. C* **2010**, *66*, o513−o516. (o) Konovalova, I. S.; Nelyubina, Y. V.; Lyssenko, K. A.; Paponov, B. V.; Shishkin, O. V. *J. Phys. Chem. A* **2011**, *115*, 8550−8562.
(20) (a) Morokuma, K. *J. Chem. Phys.* **1971**, *55*, 1236. (b) Kitaura, K.; Morokuma, K. *Int. J. Quantum Chem.* **1976**, *10*, 325. (c) Chałasinski, G.; Szczesniak, M. *Chem. Rev.* **1994**, *94*, 1723. (d) Sokalski, W. A.; Roszak, S.; Pecul, K. *Chem. Phys. Lett.* **1988**, *153*, 153. (e) Cybulski, S. M.; Chałasinski, G.; Moszynski, R. J. *Chem. Phys.* **1990**, *92*, 4357.
(21) (a) Szalewicz, K. *WIREs Comput. Mol. Sci.* **2012**, *2*, 254−272. (b) Cybulski, H.; Sadlej, J. *J. Chem. Theory Comput.* **2008**, *4*, 892−897. (c) Jeziorski, B.; Moszyn.ski, R.; Szalewicz, K. *Chem. Rev.* **1994**, *94*, 1887.
(22) (a) Espinosa, E.; Molins, E.; Lecomte, C. *Chem. Phys. Lett.* **1998**, *285*, 170−173. (b) Espinosa, E.; Alkorta, I.; Rozas, I.; Elguero, J.;

Molins, E. *Chem. Phys. Lets.* **2001**, *336*, 457−464. (c) Mata, I.; Alkorta, I.; Espinosa, E.; Molins, E. *Chem. Phys. Lett.* **2011**, *507*, 185−189.
(23) Otwinowski, Z.; Minor, W. *Methods Enzymol.* **1997**, *276*, 307−326.
(24) (a) Zhurova, E. A.; Zhurov, V. V.; Tanaka, K. *Acta Crystallogr., Sect. B* **1999**, *55*, 917−922. (b) Zhurov, V. V.; Zhurova, E. A.; Pinkerton, A. A. *J. Appl. Crystallogr.* **2008**, *41*, 340−349.
(25) (a) Blessing, R. H. *Acta Crystallogr., Sect. A* **1995**, *51*, 33−38. (b) Blessing, R. H. *J. Appl. Crystallogr.* **1997**, *30*, 421−426.
(26) Sheldrick, G. M. *SHELXS97*; University of Gottingen: Germany, 1997.
(27) Sheldrick, G. M. *Acta Crystallogr., Sect. A* **2008**, *64*, 112−122.
(28) Hansen, N. K.; Coppens, P. *Acta Crystallogr., Sect. A* **1978**, *34*, 909−921.
(29) Volkov, A.; Macchi, P.; Farrugia, L. J.; Gatti, C.; Mallinson, P.; Richter, T.; Koritsanszky, T. *XD2006*, Rev. 5.34; University at Buffalo, State University of New York: Buffalo, NY, 2006.
(30) (a) Kirzhnits, D. A. *Sov. Phys. JETP* **1957**, *5*, 64−72. (b) Abramov, Yu. A. *Acta Crystallogr., Sect. A* **1997**, *53*, 264−272. (c) Tsirelson, V. G. *Acta Crystallogr., Sect. B* **2002**, *58*, 632−639.
(31) (a) Stash, A. I.; Tsirelson, V. G. *J. Appl. Crystallogr.* **2002**, *35*, 371−373. (b) Stash, A. I.; Tsirelson, V. G. *Crystallogr. Rep.* **2005**, *50*, 177−184.
(32) Dovesi, R.; Saunders, V. R.; Roetti, R.; Orlando, R.; Zicovich-Wilson, C. M.; Pascale, F.; Civalleri, B.; Doll, K.; Harrison, N. M.; Bush, I. J.; D'Arco, P.; Llunell, M. *CRYSTAL09 (CRYSTAL09 User's Manual)*; University of Torino: Torino, 2009.
(33) (a) Vener, M. V.; Sauer, J. *Phys. Chem. Chem. Phys.* **2005**, *7*, 258−263. (b) Zicovich-Wilson, C. M.; San-Román, M. L.; Camblor, M. A.; Pascale, F.; Durand-Niconoff, J. S. *J. Am. Chem. Soc.* **2007**, *129*, 11512−11523. (c) Jezierska, A.; Panek, J. J.; Koll, A.; Mavri, J. J. *Chem. Phys.* **2007**, *126* (205101), 1−9. (d) Vener, M. V.; Manaev, A. V.; Tsirelson, V. G. J. *Phys. Chem. A* **2008**, *112*, 13628−13632. (e) Jezierska-Mazzarello, A.; Vuilleumier, R.; Panek, J. J.; Ciccotti, G. J. *Phys. Chem. B* **2010**, *114*, 242−253.
(34) (a) Rozenberg, M.; Loewenschuss, A.; Marcus, Y. *Phys . Chem. Chem. Phys.* **2000**, *2*, 2699−2702. (b) Rozenberg, M.; Shoham, G.; Reva, I.; Fausto, R. *Phys . Chem. Chem. Phys.* **2005**, *7*, 2376−2383. (c) Musin, R. N.; Mariam, Y. H. *J. Phys. Org. Chem.* **2006**, *19*, 425−444.
(35) Iogansen, A. V. *Spectrochim. Acta. A* **1999**, *55*, 1585−1612.
(36) (a) Filarowski, A.; Koll, A.; Sobczyk, L. *Curr. Org. Chem* **2009**, *13*, 172−193. (b) Mohammadzadeh Jahani, P.; Nowroozi, A.; Hajiabadi, H.; Hassani, M. *Struct. Chem.* **2012**, *23*, 1941−1951.
(37) Lyssenko, K. A. *Mendeleev Commun.* **2012**, *22*, 1−7.
(38) (a) Borissova, A. O.; Korlyukov, A. A.; Antipin, M. Y.; Lyssenko, K. A. *J. Phys. Chem. A* **2008**, *112*, 11519−11522. (b) Nelyubina, Yu. V.; Antipin, M. Yu.; Lyssenko, K. A. *Usp. Khim.* **2010**, *79*, 195−217.
(39) Sarma, J. A. R. P.; Desiraju, G. R. *Acc. Chem. Res.* **1986**, *19*, 222−228.
(40) Steiner, T. M.; Schreurs, A. M.; Lutz, M.; Kroon, J. *Acta Crystallogr., Sect. C* **2000**, *56*, 577−579.
(41) Gatti, C.; May, E.; Destro, R.; Cargnoni, F. *J. Phys. Chem. A* **2002**, *106*, 2707−2720.
(42) Tsirelson, V. G.; Ozerov, R. P. *Electron Density and Bonding in Crystals*; Institute of Physics Publishing: Bristol, England/Philadelphia, 1996.
(43) (a) Khinchin, A. I. *Mathematical Foundations of Information Theory*; Dover: New York, 1957. (b) Ash, R. *Information Theory*; Interscience Publishers: New York, 1965.
(44) Shannon, C. E. *Bell System Techn. J.* **1948**, *27*, 379−423.
(45) (a) Nalewajski, R. F. *Information Theory of Molecular Systems*; Elsevier: Amsterdam, 2006. (b) Nalewajski, R. F. *Information Origins of the Chemical Bond*; Nova Science Publishers: New York, 2010. (c) Ihara, S. *Information Theory for Continuous Systems*; World Scientific Publishing: Singapore, 1993.
(46) Tsirelson, V.; Nagy, A. *J. Phys. Chem. A* **2009**, *113*, 9022−9029.
(47) Nguyen, T. H.; Groundwater, P. W.; Platts, J. A.; Hibbs, D. E. *J. Phys. Chem. A* **2012**, *116*, 3420−3427.
(48) Hoser, A. A.; Jarzembska, K. N.; Dobrzycki, L.; Gutmann, M. J.; Wozniak, K. *Cryst. Growth Des.* **2012**, *12*, 3526−3539.
(49) (a) Fedorov, I. A.; Zhuravlev, Y. N.; Berveno, V. P. *Phys. Chem. Chem. Phys.* **2011**, *13*, 5679−5686. (b) King, M. D.; Blanton, T. N.; Korter, T. M. *Phys. Chem. Chem. Phys.* **2012**, *14*, 1113−1116. (c) Bucko, T.; Hafner, J.; Lebegue, S.; Angyan, J. G. *J. Phys. Chem. A* **2010**, *114*, 11814−11824.
(50) Tsirelson, V.; Avilov, A.; Lepeshov, G.; Kulygin, A.; Stahn, J.; Pietsch, U.; Spence, J. C. H. *J. Phys. Chem. B* **2001**, *105*, 5068−5074.
(51) Tsirelson, V. G.; Shishkina, A. V.; Stash, A. I.; Parsons, S. *Acta Crystallogr., Sect. B* **2009**, *65*, 647−658.
(52) Mata, I.; Alkorta, I.; Molins, E.; Espinosa, E. *ChemPhysChem* **2012**, *13*, 1421−1424.
(53) Chickos, J. S.; Acree, W. E. *J. Phys. Chem. Ref. Data* **2002**, *31*, 537−698.
(54) Wendler, K.; Thar, J.; Zahn, S.; Kirchner, B. *J. Phys. Chem. A* **2010**, *114*, 9529−9536.
(55) Guin, M.; Patwari, G. N.; Karthikeyanb, S.; Kim, K. S. *Phys. Chem. Chem. Phys.* **2011**, *13*, 5514−5525.
(56) Pandey, R.; Mukhopadhyay, S.; Ramasesha, S.; Das, P. K *J. Phys. Chem. B* **2011**, *115*, 13842−13846.
(57) Hoepfner, V.; Deringer, V. L.; Dronskowski, R. *J. Phys. Chem. A* **2012**, *116*, 4551−4559.
(58) Dobado, J. A.; Molina, J.; Portal, D. *J. Phys. Chem. A* **1998**, *102*, 778−784.